Electronic supplementary materials *Mendeleev Commun.*, 2026, **36**, 101–103

CO_2 hydrogenation over catalysts based on Fe–Co double complex salts

Alevtina N. Gosteva, Mayya V. Kulikova, Sergey A. Svidersky, Alena A. Grabchak, Semen E. Lapuk and Alexander V. Gerasimov

EXPERIMENTAL

Materials

DCS $[Co(NH_3)_6]_4[Fe(CN)_6]_3 \cdot 13H_2O$ was obtained by mixing equivalent amounts of solutions of $[Co(NH_3)_6]Cl_3$ and $K_3[Fe(CN)_6]$. All reagents were purchased from Vecton.

H_2, CO and CO_2 with a purity of 99.999% were used for catalyst activation procedure and for catalytic activity testing.

Obtaining Catalytic Composition

The catalyst was the product of the thermal destruction of $[Co(NH_3)_6]_4[Fe(CN)_6]_3 \bullet 13H_2O$ in argon (99.999 weight %) at 650 °C within 1 h, at a heating rate of 10 °C/min. The tubular muffle furnace Nabertherm RT 50-250/11 (Nabertherm GmbH, Lilienthal, Germany, 2013) used.

Physicochemical Research Methods

Elemental analysis carried out using the analyzer ELTRA-2000 (Alpha Resources, LLC, Stevensville, MI, USA, 2004) and on an atomic absorption spectrometer with a hydride attachment, and a flow-through sample preparation unit for sorption concentration “Kvant-2A” (LLC Kortec, 2003, St. Petersburg, Russia).

X-ray spectral microanalysis (XMA) of the sample was performed on a ZEISS EVO scanning electron microscope (Carl Zeiss, Germany, 2018) at an accelerating voltage of 20 kV, a probe current of 2nA and a fixed operating distance of 8.5 mm using an INCA Energy 450 energy dispersive microanalyzer (OXFORD instruments, Great Britain, 2007) in the "Point&ID" mode.

Fourier transform infrared spectra were recorded with a Nicolet 6700 FT-IR spectrophotometer (Thermo Fisher Scientific Inc., Hillsboro, OR, USA, 2010) in the wavelength range of 400 cm^{-1} to 4000 cm^{-1}, with tablet KBr, 16 scans, 4 resolution cm^{-1}.

The porous structure of the samples was studied using the method of low-temperature sorption of nitrogen on a Tristar 3020 instrument (Micrometritics, Norcross, GA, USA, 2009). The X-ray phase analysis of the products of the thermal destruction of DCS was made in 2θrange 10–100° on a Shimadzu XRD 6000 powder diffractometer (Shimadzu, Kyoto, Japan, 2008), equipped with a Cu-Ka source (λ= 1.5418 Å) and a graphite monochromator for the diffracted beam. Indexing of the diffraction patterns performed using the data for pure metals and compounds reported in the JCPDS-ICDD PDF4+ database (2019).

The analysis of the products carried out on a Khromos GC-1000 gas-adsorption chromatographic complex. The detector was a katharometer, and the carrier gas was helium with 5% nitrogen as an internal standard, which supplied at a flow rate of 20 mL/min. Two columns were used for the analysis: the first column separated CO, N_2, and CH_4 gases on CaA molecular sieves under isothermal conditions at a

temperature of 80 °C, and the second column served to separate CO_2 and C_2–C_4 hydrocarbons in the temperature range of 80–200 °C and was filled with HayeSep R.

The Raman spectra obtained using a confocal Raman microscope Senterra II (Bruker, Billerica, MA, USA). A laser with a wavelength of 532 nm and a power of 0.25 mW used to excite the Raman scattering. The accumulation time was 1 sec, the number of repetitions was 200, the objective was 50X, the diffraction grating had 400 lines/mm, the resolution was 4 cm^{-1}, and the aperture was 50 × 1000 μm. Ten spectra from different selected areas recorded for each sample. Spectral processing carried out using the OPUS 8.5 software package (Bruker, Billerica, MA, USA).

The study of the composite material samples' surface carried out by X-ray photoelectron spectroscopy on an X-ray photoelectron spectrometer (Prevac, Rogow, Poland). An X-ray tube with AlKα radiation (1486.6 eV) used as a source of ionizing radiation. Before being loaded into the spectrometer, the samples were ground in an agate mortar and applied to conductive carbon tape. To neutralize the charge of the sample during the experiments, an electron-ion charge compensation system used. All peaks calibrated versus the C 1s peak at 284.8 eV. The type of background was Shirley and during deconvolution, it assumed that the total peak was the sum of Gaussian curves.

Simultaneous Thermal Analysis

Simultaneous thermal analysis (thermogravimetry (TG) and differential scanning calorimetry (DSC)) carried out using an STA 449 F1 Jupiter micro-thermoanalyzer (Netzsch, Germany). All studies carried out in an argon atmosphere with a flow rate of 75 ml/min a heating rate of 1, 5, 10 and 20 °C/min. The measurements taken in the temperature range from 40 to 1000 °C. For experiments, 10–20 mg samples placed in Al_2O_3 crucibles (40 μL) with lids having one hole of 0.5 mm in diameter.

Kinetic analysis

Kinetic parameters were calculated using both model-based and isoconversional approach-es. In the work, Friedman's analysis and the method KAS were used to calculate the activation energy of thermolysis using isoconversion approaches.

Model methods are based on the determination of kinetic parameters by minimizing the difference between empirical and theoretical values. The minimization was carried out using lin-ear regression methods. The evaluated models include n-dimensional nucleation according to re-action of nth order (Fn), Avrami-Erofeev (An), reaction of nth order with m-power autocatalysis by product (Cnm), expanded Prout-Tompkins equation (Bna) and expanded Sestak-Berggren equation (Sb). The kinetic parameters of thermolysis were determined based on the different heating rates. Kinetic analysis was performed according to the ICTAC recommendations using NETZSCH Kinetics Neo 2.1.2.2 software package.

Catalytic Tests

Catalytic tests were carried out in the temperature range from 230 °C to 310 °C, with a step of 20 °C and exposure for 12h for each temperature, at a pressure of 2.0 MPa in a flow unit with a fixed catalyst bed, gaseous reagents (H_2:CO_2 = 3:1) and space velocity of 1500 h^{-1}. Catalytic tests carried out at the stage of preliminary activation of the sample with hydrogen or carbon monoxide at a temperature of 450 °C for 1 h, pressure of 2.0 MPa, and the gas space velocity of 1000 h^{-1} or without the stage of preliminary activation. If the activation used, after activation the reactor was cooled to 230 °C and gaseous reactants (H_2:CO_2 = 3:1) were fed into the reactor at 2.0 MPa and space velocity of 1500 h^{-1}.

The efficiency of the tested system evaluated from the calculation of output indicators: CO_2 conversion and selectivity.

CO_2 conversion is the ratio of the mass of reacted CO_2 to the mass of carbon dioxide that entered in the reaction zone (1):

$$Xco_2 = \frac{M_{CO_2}^{reacted}}{M_{CO_2}^{entered}} \cdot 100\% \quad (1)$$

The selectivity of the formation of products is the ratio of the amount of product formed to the amount of reacted raw materials (2):

$$S = \frac{M_{products}}{M_{CO2}^{reacted}} \cdot 100\% \quad (2)$$

The specific activity–metal time yield (MTY, A) of a catalyst is the number of reacted moles of CO_2 per gram of Fe-Co per second (3):

$$A = \frac{N_{co2}}{M_{Fe-Co} \cdot t} \quad (3)$$

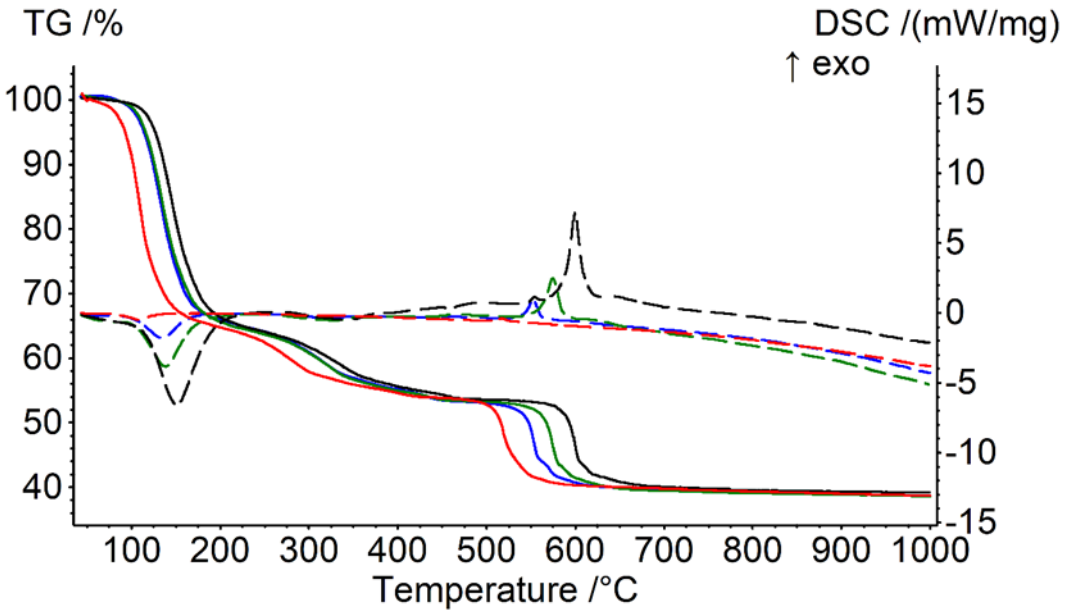

Figure S1. DCS 4/3 MET sample, witch formation by thermolysis:
TG/DSC curves for heating $[Co(NH_3)_6]_4[Fe(CN)_6]_3 \cdot 13H_2O$at speeds of 1, 5, 10 and 20 °C/min. All studies conducted in an argon atmosphere with a flow rate of 75 ml/min. The red curve is 1 K/min, the blue curve is 5 K/min, the green curve is 10 K/min, and black curve is 20 K/min.

The DCS 4/3 thermolysis process is divided into two stages. The 1 stage is from 100 to 450°C and the 2 stage is above 500°C. The thermolysis process is complex and multi-stage, and the stages are grouped for kinetic analysis.

The activation energies and pre-exponential multipliers of the 1 and 2 stages of DCS 4/3 thermolysis depending on the degree of conversion were determined using isoconversion approaches, namely Friedman analysis and the KAS (Kissinger–Akahira–Sunose) method. The dependences of the activation energy on the degree of conversion have a sharp inflection at 70% conversion. This may indicate two successive reactions in the first and second stages of thermolysis. Table S1 and Figure S2 show the

average values of the kinetic parameters for each process. The data were determined using isoconversion approaches.

The kinetic parameters determined using model methods are consistent with those calculated using isoconversion approaches. All stages of the first two thermolysis stages can be described by autocatalytic models. This indicates a catalytic mechanism of the process.

When the ratio of DCS central atoms was increased from $[Co(NH_3)_6][Fe(CN)_6]$ (DCS 1/1) [18] to DCS 4/3, it significantly affected the kinetics of stages 1 and 2 of thermolysis. The activation energy of the first stage of thermolysis of DCS 4/3 changes abruptly from 100 to 250 kJ/mol, in contrast to this, the activation energy of thermolysis was 130 kJ/mol for DCS 1/1. The second stage for DCS 1/1 is characterized by a higher activation energy of the thermolysis process. This means that an increase in the ratio of the central atoms of DCS can lead to a slowdown in the first stage of thermolysis and an acceleration of the second stage.

(a)

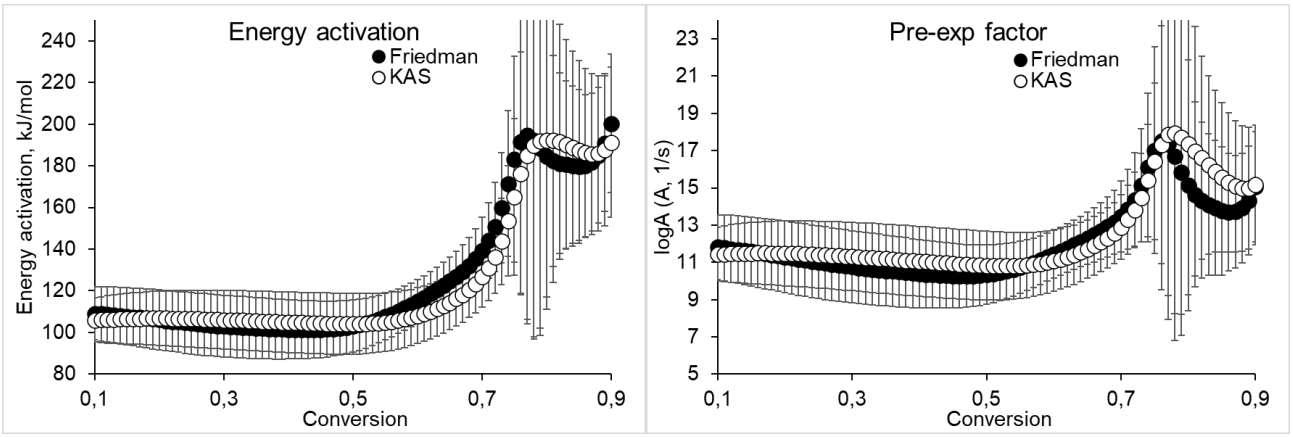

(b)

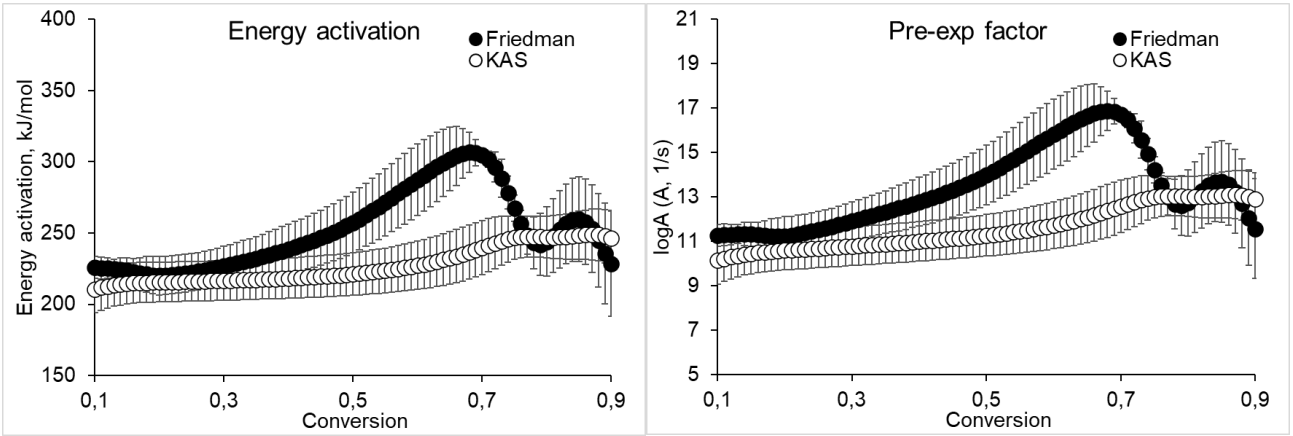

Figure S2. DCS 4/3 MET sample, witch formation by thermolysis:
Dependences of the activation energy and the pre-exponential multiplier on the degree of conversion, determined using Friedman analysis and the KAS method for the first (a) and the second (b) stages of $[Co(NH_3)_6]_4[Fe(CN)_6]_3 \cdot 13H_2O$thermolysis.

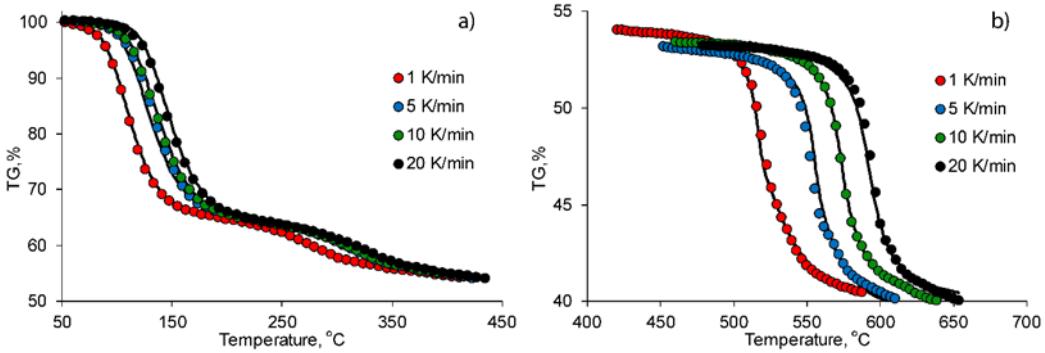

Figure S3. DCS 4/3 MET sample, witch formation by thermolysis:
TG/DSC curves, approximated by equations (Table 3) of model methods for the first (a) and the second (b) stages of $[Co(NH_3)_6]_4[Fe(CN)_6]_3 \cdot 13H_2O$thermolysis.

A number of modeling methods were used to determine the kinetic parameters of DCS 4/3 thermolysis. Model-based approaches provide greater accuracy. Two-stage models were used based on kinetic data. The TG/DSC curves fitted by the equations (Table S2) of the model methods are shown in figure S3 (see Supplementary Material online). See table S2 for the models with the highest coefficient of determination. The kinetic analysis of DCS 4/3 thermolysis is presented in Tables S1–S4. Data for DCS 1/1 are given in[18]. Tables S3 and S4 contain the key results of the kinetic parameter modeling. The results were obtained using non-isothermal kinetic approaches. They confirm the autocatalytic nature of the process and are necessary to justify the choice of models in table S2.

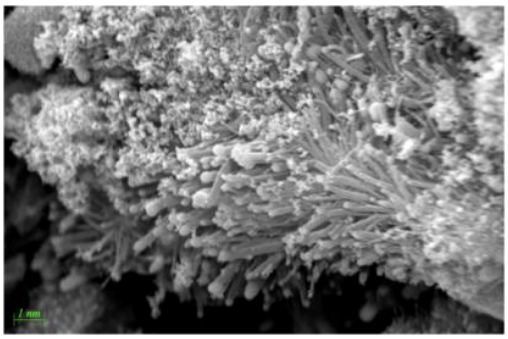

Figure S4. Photomicrograph of DCS 4/3 MET

According to the microprobe analysis, it was established that the DCS 4/3 MET sample is represented by hollow carbon tubes. The balls of the intermetallic compound Co_4Fe_3 are located at the ends of these tubes. The DCS 4/3 MET sample has a structure close to DCS 1/1 HC. The structure differs only in the composition of the intermetallic compound CoFe.

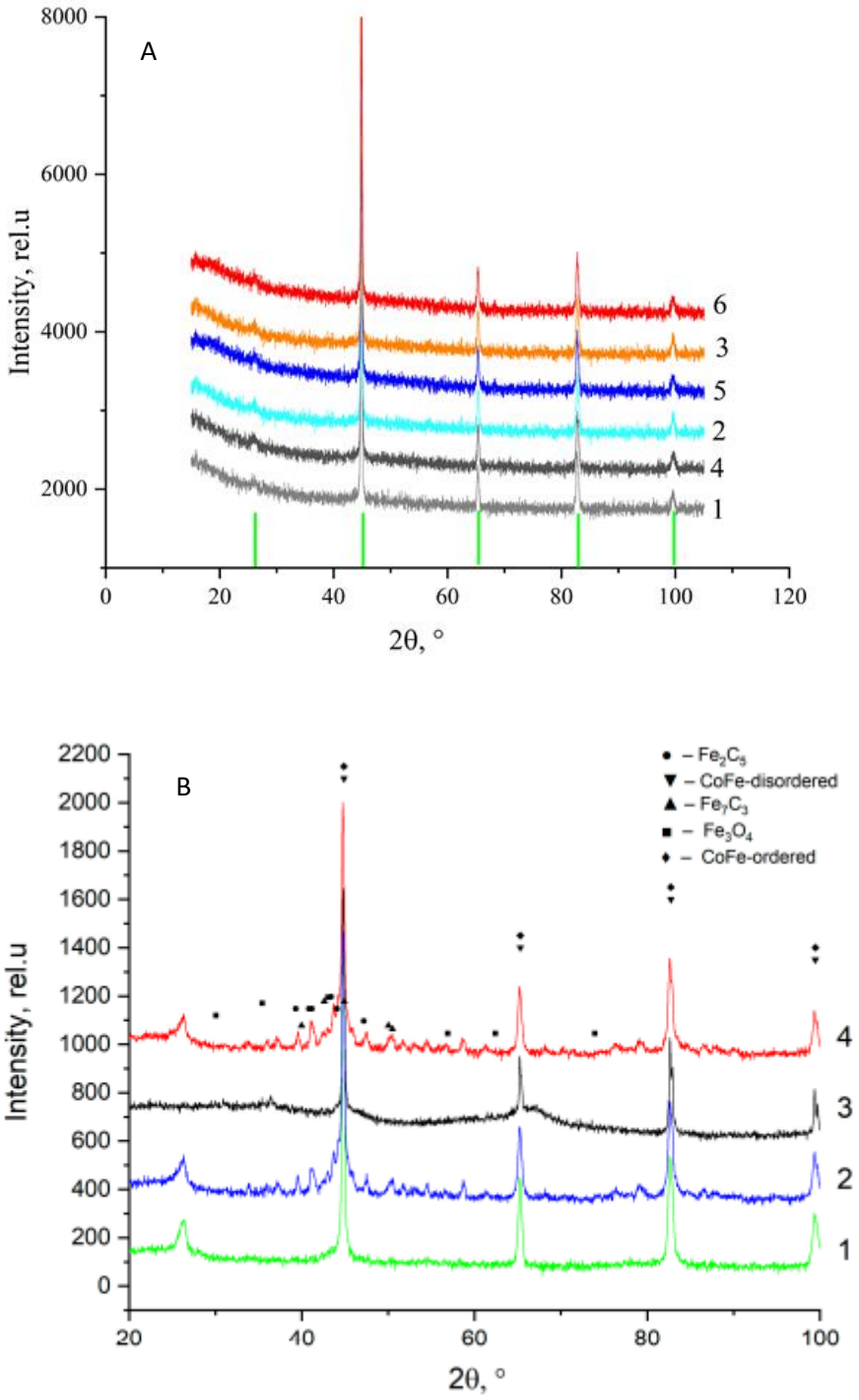

Figure S5. A) X-ray diffraction patterns of DCS 4/3 MET samples before CO_2 hydrogenation (non-activated catalyst (1), H_2-activated (2), CO-activated (3)) and after CO_2 hydrogenation (non-activated catalyst (4), H_2-activated (5), CO-activated (6)); | - marcs of FeCo alloy characteristic peaks.
B) (Cited by [S1]) X-ray diffraction pattern of DCS 1/1 HC: 1—precursor sample after hydrogen treatment; 2—precursor sample after hydrogen treatment and catalytic experiment; 3—precursor sample; 4—precursor sample after catalytic experiment.

The main crystallized phase was CoFe alloy in an ordered state for all samples (PDF database#49-1567). The surface of active centers promotes a deeper reaction of water conversion into gas in this state. The reverse reaction of the water shift reaction that occurs on the iron-containing fragments results in the formation of carbon monoxide. Carbon monoxide is adsorbed on the cobalt-containing fragment of the

particle and then hydrogenated predominantly to methane. Other phases active in the hydrogenation process, such as carbides Fe_7C_3 (database JCPDS-75-1499) and χ-Fe_5C_2 (database JCPDS-51-0997), and Fe_3O_4 (database JCPDS-79-0419), can also be found on the sample surface in small quantities, but their contribution to the catalytic process was significantly less than for the FeCo alloy. These phases provided activity in the polymerization process of intermediate products, and the intermediate products lead to the formation of C_{2+} hydrocarbons.

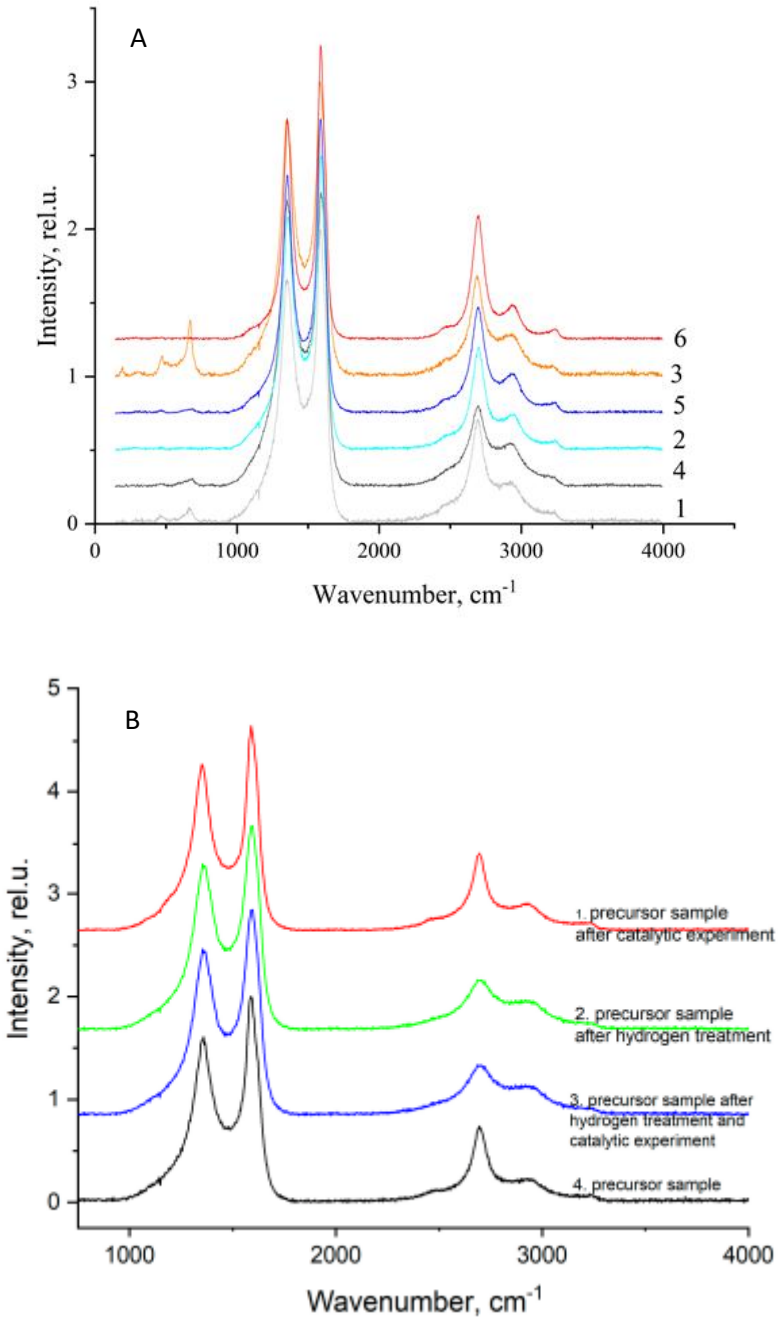

Figure S6. A) Raman spectra of DCS 4/3 MET samples before CO_2 hydrogenation (non-activated catalyst (1), H_2-activated (2), CO-activated (3)) and after CO_2 hydrogenation (non-activated catalyst (4), H_2-activated (5), CO-activated (6);
B) (Cited by [S1]) Raman-spectra of DCS 1/1 HC: 1— precursor sample after catalytic experiment; 2—precursor sample after hydrogen treatment; 3—precursor sample after hydrogen treatment and catalytic experiment; 4—precursor sample.

The intensity ratio of D and G bands (ID/IG) can reflect the relative amount of graphitic structure and disordered structure in carbon components [S2]. It can be seen that for DCS 4/3 MET this ratio does not depend on the activation conditions and CO_2 hydrogenation and is about 0.8. This indicates a high degree of ordering of the graphitization and, in contrast to the data for DCS 1/1 HC [S1], does not increase during the catalytic tests. The second-order bands in the range from 2457 to 3000 cm^{-1} associated with the combination of 2D, G' and D + G modes/overtones may indicate the presence of single-walled carbon nanotubes and low-layer graphene in the structure [S3], but they also do not show any changes after sample activation and catalytic testing.

Table S1. DCS 4/3 MET sample, witch formation by thermolysis:
Average values of kinetic parameters of the $[Co(NH_3)_6]_4[Fe(CN)_6]_3 \cdot 13H_2O$ thermolysis process.

Isoconversion approach		Stage 1		Stage 2	
		Step 1	Step 2	Step 1	Step 2
Friedman's Analysis	Activation Energy E, kJ/mol	110	250	240	260
	The pre-exponential multiplier lgA (A, 1/s)	11.2	19.7	12.8	13.5
KAS technique	Activation Energy E, kJ/mol	110	230	220	250
	The pre-exponential multiplier lgA (A, 1/s)	11.3	19.0	11.0	13.0

Table S2. A. DCS 4/3 MET sample, witch formation by thermolysis:
Kinetic parameters of the first and second stages of $[Co(NH_3)_6]_4[Fe(CN)_6]_3 \cdot 13H_2O$ above-ground thermolysis using model approaches.

Material	Stage 1		Stage 2	
	Step 1	Step 2	Step 1	Step 2
	Fn	Sb	Cnm	Sb
DCS 4/3	E=104.5 kJ/mol logA=11.5 (A, 1/s) Reactorder n=2,6	E=134.4 kJ/mol logA=10.0 (A, 1/s) Reactorder n=4,5 Autocat Order 0,01 LogOrder q=0,01	E=223.1 kJ/mol logA= 11.3 (A, 1/s) Reactorder n=1 Log(AutocatPreExp) 1.5 Autocat Power m=3.0	E=311.8 kJ/mol logA=17.6 (A, 1/s) Reactorder n=2.9 Autocat Order 0.03 LogOrder q=0.4
	R^2			
	0.99950		0.99865	

Table S2. B. (Cited by [S1]) DCS 1/1 HC sample Kinetic parameters of the $[Co(NH)_3]_6][Fe(CN)_6]$ thermolysis determined by using model methods.

The first stage		The second stage
The first reaction	The second reaction	
Cnm	Sb	Cnm
E=127.3 kJ/mol logA= 11.1 (A, 1/s) Reactorder n=1.2 Log(AutocatPreExp) 0.4 Autocat Power m=0.8	E=77.6 kJ/mol logA=4.8 (A, 1/s) Reactorder n=3.7 Autocat Order 0.4 LogOrder q=0.8	E=345.7 kJ/mol logA= 18.2 (A, 1/s) Reactorder n=2.8 Log(AutocatPreExp) 1.6 Autocat Power m=1.7
R^2		
0.99957		0.99928

Table S3. Model methods for calculating kinetic parameters.

Model	Equation
Fn	$f = (1-\alpha)^n$
An	$f = n * (1-\alpha) * [-\ln(1-\alpha)]^{(n-1/n)}$
Bna	$f = (1-\alpha)^n * \alpha^{AutocatOrder}$
Cnm	$f = (1-\alpha)^n * (1+AutocatOrder) * \alpha^m$
Sb	$f = (1-\alpha)^n * \alpha^m * [-\ln(1-a)]^q$

Table S4. Components of DCS-based samples.

Sample index	Target product	Co, wt %	Fe, wt %	C, wt %
DCS 4/3 MET	Methane	40.1	29.7	22.4
DCS 1/1 HC	C_{5+}hydrocarbons	35.8	32.1	25.4

References

S1. N. Gosteva, M. V. Kulikova, M. I. Ivantsov, A. A. Grabchak, Y. P. Semushina, S. E. Lapuk, A. V. Gerasimov and N. S. Tsvetov, *Catalysts*, 2023, **13**, 1475; https://doi.org/10.3390/catal13121475.

S2. B. Guo, G. Song, M. Chen, H. Yu, M. Ran, H. Wang, B. Yu, Z. Ma, J. Chen, M. Wang and X. Li, *Surf. Interfaces*, 2023, **42**, 103419; https://doi.org/10.1016/j.surfin.2023.103419.

S3. B. Ma, R. D. Rodriguez, A. Ruban, S. Pavlov and E. Sheremet, *Phys. Chem. Chem. Phys*., 2019, **21**, 10125; https://doi.org/10.1039/C9CP00093C.